frontiers | Frontiers in Immunology

TYPE Original Research
PUBLISHED 13 August 2025
DOI 10.3389/fimmu.2025.1626888

OPEN ACCESS

EDITED BY
Cyrus Khandanpour,
Klinik für Hämatologie und Onkologie,
Germany

REVIEWED BY
Christian H. K. Lehmann,
University Hospital Erlangen, Germany
Cong Wang,
Jilin University, China

*CORRESPONDENCE
Feifei Yang
lydia9017@163.com
Xuezhong Zhang
njfh803@aliyun.com
Guoguang Zheng
zhengggtjchn@aliyun.com

†These authors contributed equally to this work and share senior authorship

RECEIVED 12 May 2025
ACCEPTED 28 July 2025
PUBLISHED 13 August 2025

CITATION
Yang F, Luo S, Yang D, Cui X, Zhang D, Wang H, Li Y, Xie W, Wang L, Zhang X, Zheng G and Zhang X (2025) Iron overload promotes myeloid differentiation of normal hematopoietic stem cells and educates macrophage mediated immunosuppression in acute myeloid leukemia.
Front. Immunol. 16:1626888.
doi: 10.3389/fimmu.2025.1626888

Iron overload promotes myeloid differentiation of normal hematopoietic stem cells and educates macrophage mediated immunosuppression in acute myeloid leukemia

Feifei Yang[1*], Shulin Luo[1], Dan Yang[1], Xiaoxi Cui[2], Dongyue Zhang[2], Hao Wang[2], Yifei Li[2], Wanzhen Xie[2], Lina Wang[2,3], Xiuqun Zhang[1], Guoguang Zheng[2,3*†] and Xuezhong Zhang[1*†]

[1]Nanjing First Hospital, Nanjing Medical University, Nanjing, China, [2]State Key Laboratory of Experimental Hematology, National Clinical Research Center for Blood Diseases, Haihe Laboratory of Cell Ecosystem, Institute of Hematology & Blood Diseases Hospital, Chinese Academy of Medical Sciences & Peking Union Medical College, Tianjin, China, [3]Tianjin Institutes of Health Science, Tianjin, China

Background: The hematopoietic ecosystem comprises both cellular components such as hematopoietic stem cells (HSCs) and immune cells as well as non-cellular components including iron. Systemic iron overload, which leads to serious complications and affects both patients' quality of life and overall survival, is a common clinical challenge in patients with acute myeloid leukemia (AML). We previously elucidated the direct effects of iron overload on AML cells. It's worth noting that iron overload remodels the hematopoietic ecosystem. However, whether and how remodeled leukemic microenvironment with overloaded iron regulates normal HSCs and immune cells, especially leukemia-associated macrophages (LAMs), in AML have not been elucidated.

Methods: The MLL-AF9-induced AML (MA9) cells were originated from c-kit$^+$ BM cells enriched from C57BL/6J mice that infected with MSCV-MLL-AF9-GFP retrovirus. The MA9 AML mouse model was established by transplantation of MA9 cells into C57BL/6 mice. MA9 mice were *i.p.* administered with iron dextran every other day for a total of 6 times to established the iron overload MLL-AF9-induced AML mouse model (MA9/FE). HSC maintenance and differentiation was assessed by flow cytometry, cell proliferation, cell apoptosis, colony forming and competitive transplantation assays. LAM activation and function was analyzed by RNA-sequencing, flow cytometry and coculture assay. Intravenous clodronate liposome administration was employed to reduce LAMs in AML.

Results: Iron overload skewed myeloid differentiation of normal HSCs. Furthermore, iron overload affected LAMs in the AML microenvironment by promoting LAM polarization toward an M2 phenotype. Functionally, iron overload decreased the phagocytic function of LAMs against leukemia cells and inhibited LAM-induced T cell activation by acquiring a tolerogenic phenotype with aberrant immune checkpoints. Moreover, depletion of LAMs attenuated iron overload caused acceleration of AML progression.

Conclusions: Collectively, this study reveals the significance of iron overload in remodeling hematopoietic ecosystem and affecting HSC and LAM function in AML, providing new insights into the multifaceted role of iron overload in leukemia.

KEYWORDS

acute myeloid leukemia, iron overload, myeloid differentiation, leukemia-associated macrophages, immunosuppression

Introduction

Iron is an essential element involved in numerous fundamental intracellular and extracellular physiologic processes. Iron homeostasis disorders play vital roles in the pathophysiology of various diseases as they cause diverse functional changes and progressive damages to organs (1–5). The relationship between the dysregulation of iron metabolism and the occurrence and progression of hematologic diseases has been reported (6). Acute myeloid leukemia (AML) is a hematologic malignancy characterized by the unlimited proliferation of myeloid precursor cells in the bone marrow (BM) with poor outcome although great progress has been achieved (7, 8). Iron overload reshapes the microenvironment, which has adverse effects on the initiation and progression of AML. Elevated iron promotes myelodysplastic syndromes (MDS)-AML transformation by causing genetic and chromosomal abnormalities (9), which could be attenuated by the treatment of iron chelators (10). Clinical studies have revealed that a high iron level is associated with a suppressed autologous stem cell mobilization, a poorer overall survival, and a higher incidence of relapse in AML patients (11–13). Our previous work demonstrated that the high level of iron correlated with a worse prognosis in AML patients and a shortened survival time in AML mice (14). Although we previously demonstrated that iron overload directly regulated AML cells by decreasing leukemic stem cells (LSCs) levels but increasing the tumor load in BM and extramedullary tissues via promoting the proliferation of leukemia cells through the upregulation of *FOS* (14), a comprehensive interpretation of the pathologic roles of iron overload in leukemia, especially the crosstalk between iron overload leukemic microenvironment and normal hematopoietic components, is less well-defined.

Leukemia cells highjack and destroy microenvironments, potentially shifting the equilibrium of microenvironments from a state that supports steady-state hematopoiesis to the conditions in favor of leukemogenesis and progression. Multiple types of cells including leukemia cells themselves (15, 16), normal hematopoietic cells (17, 18), immune cells (19), *etc.* are affected and contribute to the process. Hematopoietic stem cells (HSCs) are unique and hierarchically organized subpopulations of blood cells that maintain the hematopoietic system through self-renewal and generation of progenitor cells and mature cells of various lineages through differentiation in response to physiologic demands (20). Previous work demonstrated that leukemic microenvironment exhibited a great impact on HSCs as well as normal hematopoiesis (17, 18). However, iron overload further remodels the leukemic microenvironment. Evidence has suggested that iron may play important roles in hematopoiesis under steady state and stress conditions. Microbiota, antifungal agents, or transferrin receptor 1 (Tfr1)-mediated iron uptake have been shown to regulate HSC fate decisions in the BM (21–23). F-box and leucine-rich repeats protein 5 (FBXL5) or ferritin heavy chain 1 (*FTH1*)-mediated cellular iron homeostasis is required for the maintenance of HSCs functions (19, 24). In addition, the increased iron uptake by splenic HSCs has been shown to promote TET2-dependent erythroid regeneration in hemolytic anemia-induced stress erythropoiesis. However, how remodeled leukemic microenvironment with overloaded iron affect HSCs has not been elucidated.

The immunomicroenvironment constituted by mature immune cells and immune regulatory molecules participates in diverse physiologic and pathologic processes. Specifically, leukemia cells induce a leukemic immunomicroenvironment with suppressed immune response to leukemia cells, thereby impairing the anti-leukemia immunity, which in turn contributes to leukemia progression. Evidence demonstrated that a variety of immune cells including neutrophils (25), macrophages (26), NK cells (27, 28) and T cells (29), were reprogramed to have leukemia-associated characteristics and played pathologic roles. It is worth noting that leukemia-associated macrophages (LAMs) were educated by the leukemic microenvironment to exhibit unique phenotypes and functions with great heterogeneity in our previous studies (30–32), highlighting a context- and tissue-dependent macrophage polarization. However, the leukemic microenvironment becomes a highly dynamic structure remodeled by iron overload. It was reported that iron played important roles on the polarization and function of macrophages under distinct conditions, including *in vitro* cytokine stimulation and some *in vivo* disease models, such as infection, metabolic disorders, and solid cancers (33–38). Nevertheless, how remodeled leukemic microenvironment with overloaded iron reshapes LAMs has not been elucidated.

In this study, we investigated the impacts of the remodeled leukemic microenvironment with overloaded iron on HSCs and immune cells by using an iron overload MLL-AF9-induced mouse AML model. The results demonstrated that iron overload skewed myeloid differentiation of normal HSCs. Furthermore, iron overload promoted LAMs to exhibit a phenotype with increased M2-related characteristics, decreased phagocytotic potential and enhanced immunosuppression ability. Moreover, depletion of LAMs attenuated iron overload-caused acceleration of AML progression. Therefore, our findings provide new insights into the mechanisms how iron overload exerts adverse effects in AML and broaden our knowledge of the multifaceted roles of iron overload in malignancies.

Materials and methods

Gene expression datasets

Public datasets of leukemia patients were downloaded from The Cancer Genome Atlas (TCGA). The correlation between gene expressions of *FTH1* or *FTL* and *CD68* or *CD163* in AML patients was studied. The detailed characteristics of the patients accessible from the database are summarized in Supplementary Table S1.

Mice

Six to eight week-old C57BL/6J (CD45.2) and B6.SJL (CD45.1) mice were provided by the Animal Centre of the Institute of Hematology and Blood Diseases Hospital, CAMS & PUMC. Mice were maintained in SPF-certified facilities, and all procedures for animal experiments were approved by the Animal Care and Use Committees at the Institution.

AML mouse models

The establishment of MLL-AF9-induced AML mouse model (MA9) was previously described (17, 39). Briefly, c-kit$^+$ BM cells were enriched from C57BL/6J mice and infected with MSCV-MLL-AF9-GFP retrovirus before transplantation into C57BL/6 mice.

We recently established the iron overload MLL-AF9-induced AML mouse model (abbreviated as MA9/FE) (14). Briefly, GFP$^+$ AML cells were isolated from MA9 mice and transplanted into C57BL/6 mice. One week after transplantation, the recipient AML mice were *i.p.* administered with 0.2 mL iron dextran (Pharmacosmos A/S, Denmark) at a concentration of 25 mg/mL every other day for a total of 6 times. An equal volume of phosphate-buffered saline (PBS) was administrated to the control AML mice (also abbreviated as MA9). C57BL/6 mice without AML cell transplantation were *i.p.* administered with an equal volume of iron dextran or PBS (abbreviated as WT/FE or WT).

Cell culture

All cells were cultured in RPMI-1640 supplemented with 5% fetal bovine serum (FBS) and antibiotics in a humidified atmosphere of 5% CO_2 at 37°C. All culture supplies were endotoxin free.

Antibodies

Fluorescence-conjugated antibodies against F4/80 (APC) and Ki67 (PE) and were purchased from BD Biosciences (USA). Fluorescence-conjugated antibodies against CD45.2 (PE), CD45.2 (PerCP-Cy5.5), Sca-1 (APC), CD117/c-Kit (PE-Cy7), CD16/32 (PerCP-Cy5.5), CD34 (BV421), Flt3 (PE), CD3 (PerCP-Cy5.5), CD4 (PE-Cy7), CD8 (APC-Cy7), CD19 (PE), CD25 (FITC), CD44 (APC), Mac-1/CD11b (PE-Cy7), Gr-1 (PE-Cy7), Gr-1 (Pacific blue), CD115 (BV711), CD115 (PE), CD47 (APC), SIRPα(APC-Cy7), PD-L1 (PE-Cy7), PD-1 (BV421), CD200 (PE-Cy7), CD200R (FITC), Galectin-9 (PerCP-Cy5.5), Tim-3 (PerCP-Cy5.5) and Annexin V (PE) were purchased from Biolegend (USA).

Flow cytometric analysis and cell sorting

EasySep^{TM} Mouse Hematopoietic Progenitor Cell Isolation Kit (#19856, Stem Cell Technologies, USA) was used to enrich the Lin$^-$ cells from the mouse BM. Lin$^-$ cells were enriched by using streptavidin-coated magnetic particles and biotinylated antibodies (CD5, CD11b, CD19, CD45R/B220, Gr-1 and Ter119, 7-4; APC-Cy7 conjugated) to remove non-hematopoietic stem/progenitor cells (HSPCs). Then, LSK$^+$ cells were gated as Lin$^-$Sca1$^+$c-Kit$^+$ from the GFP$^-$ population. Antibodies against CD34 and Flt3 were used to identify CD34$^-$Flt3$^-$ LT-HSC, CD34$^+$Flt3$^-$ ST-HSC and CD34$^+$Flt3$^+$ MPP from the GFP$^-$Lin$^-$Sca1$^+$c-Kit$^+$ population. CD34 and CD16/32 antibodies were used to identify CD34$^+$CD16/32$^+$ GMP, CD34$^+$CD16/32$^-$ CMP and CD34$^-$CD16/32$^-$ MEP from the GFP$^-$Lin$^-$Sca1$^-$c-Kit$^+$ population. These HSPCs were used for further analysis. The BM macrophages were gated as the Gr-1^{lo}F4/80$^+$CD115^{int}SSC$^{int/lo}$ subpopulation from the GFP$^-$ population. Canto II and LSR II flow cytometers (BD Biosciences) were used for FACS analysis. FACS Aria III (BD Biosciences) was used for cell sorting. Data analysis was carried out using FlowJo software (version 7.6.1).

Cell proliferation assay

Ki67 staining assays were used to detect cell proliferation of primary LSKs. Normal LSKs from MA9 and MA9/FE mice were fixed and permeabilized by Cytofix/Cytoperm^{TM} Fixation/Permeabilization Solution Kit (BD Biosciences, San Jose, CA) according to the manufacturer's protocols. Then, cells were stained with an anti-Ki67-PE antibody, followed by Hoechst 33342 before FACS analysis.

Cell apoptosis analysis

Annexin V/PI staining assay was used to detect cell apoptosis of primary LSKs. Normal LSKs from MA9 and MA9/FE mice were prepared and washed twice with pre-cold PBS buffer. Then, cells were incubated with an Annexin V-PE antibody, followed by PI before FACS analysis.

Colony forming assay

Freshly sorted normal LSKs from MA9 and MA9/FE mice were suspended in M3434 complete medium (Stem Cell Technologies, USA) and seeded in 24-well plate at 500 cells/500 µl/well and cultured according to the manufacturer's instructions. The number of burst-forming unit erythroid (BFU-E), colony-forming unit granulocyte-macrophage (CFU-GM), and colony-forming unit granulocyte, erythroid, macrophage, and megakaryocyte (CFU-GEMM) was counted on day 8.

Transplantation assays

For competitive LSK transplantation, normal LSKs (CD45.2, 1×10^3) from MA9 or MA9/FE mice and WT competitor cells (whole bone marrow cells (WBMCs)) (CD45.1, 5×10^5) were transplanted into lethally irradiated (9.5 Gy) recipient B6.SJL mice (CD45.1). The reconstitution of PB cellularity was analyzed by FACS every four weeks post-transplantation. Sixteen weeks after transplantation, BM cells from the recipient mice were collected, and the chimera rate of the HSPC compartment and lineage contribution was evaluated by FACS.

Latex bead uptake experiments

Latex bead uptake experiments were used to measure the phagocytic activity of macrophages. Prior to FACS analysis, BM macrophages from WT, WT/FE, MA9 or MA9/FE mice were incubated with FITC-labeled 2 µm latex beads (Sigma-Aldrich, USA) for 15 mins.

Phagocytotic activity of macrophages against leukemia cells

Coculture assays were used to test the phagocytosis of leukemia cells by macrophages. BM macrophages from WT, WT/FE, MA9 or MA9/FE mice were cocultured with GFP^+ BM AML cells at the ratio of 1:2 in 24-well plates for 18 hrs. Leukemia cells cultured alone were used as blank controls. After 18 hrs, total cells were counted by hemocytometer and the proportion of GFP^+ cells was analyzed by FACS (18 hrs (test)). The phagocytotic rate was calculated as follows: (100%- test) - (100%- blank control test).

Regulatory effect of macrophages on T cell activation

Co-culture assays were used to test the regulatory effects of macrophages on T cells. BM macrophages from WT, WT/FE, MA9 or MA9/FE mice were co-cultured for 48 hrs with T cells that were sorted from the spleen of normal mice, at the ratio of 1:1 in 48-well plates in the presence of Dynabeads Mouse T-Activator CD3/CD28 (Gibco, USA). Then, the cells were harvested and resuspended in 100 µl PBS. After staining with antibodies at 4°C and washing with PBS, the cells were analyzed by FACS.

Quantitative real-time PCR

Cells were lysed and total RNA was isolated using RNeasy Mini Kit (Qiagen, Valencia, CA). Reverse transcription was achieved using Transcript All-in-one First-Strand cDNA Synthesis SuperMix (TransGen Biotech, China). qRT-PCR was performed on 0.1-QuantStudio 5 and 0.2-QuantStudio 5 (Thermo Fisher Scientific, USA). The expression level of each gene was normalized to the expression level of GAPDH. Sequences for primers are listed in Supplementary Table S2.

RNA-seq

BM macrophages were sorted from WT, WT/FE, MA9 and MA9/FE mice by FACS. An RNA sequencing library was prepared and sequenced using an Illumina Nova Seq 6000 by the Beijing Novogene following standard protocols. The data was analyzed by Beijing Novogene and is available in the NCBI's Gene Expression Omnibus under the accession number GSE226727.

Two-dimensional illustration of macrophage phenotypes

A two-dimensional illustration was established to describe the activation phenotype of macrophages (31). For each gene, the value of macrophage from WT BM was designated as 0. The M1 and M2 values of macrophages were calculated and the mean values of relative expression of genes were used for calculation:

$$M1\ value=\sum\max(-\Delta\Delta CtM1,0) - \sum\min(-\Delta\Delta CtM2,0);$$

$$M2\ value=\sum\max(-\Delta\Delta CtM2,0) - \sum\min(-\Delta\Delta CtM1,0).$$

Statistical analysis

The statistical analyses were performed using the GraphPad Prism 6.0 software (San Diego, CA) and the SPSS17.0 software package (SPSS, Chicago, IL). All data were expressed as the mean ±

SEM and statistical significance was calculated using an unpaired Student's *t*-test (two groups) or one-way ANOVA (≥ three groups). Kaplan–Meier analysis was employed to compare the survival time. $P < 0.05$ was considered statistically significant.

Results

Iron overload affects normal HSC functions in AML mice

To determine the impacts of iron overload on normal HSCs in AML, the iron overloaded MLL-AF9-induced AML mouse model was successfully established and iron overload was validated (Supplementary Figure S1). The frequency of $GFP^-Lin^-c\text{-}Kit^+Sca1^+$ cells (normal LSK) in the BM of MA9 and MA9/FE mice was analyzed, and no statistical difference was detected between the two groups (Figure 1A). Then, CD34 and Flt3 were used to identify the HSC subpopulations, *i.e.* $CD34^-Flt3^-$ LT-HSC, $CD34^+Flt3^-$ ST-HSC and $CD34^+Flt3^+$ MPP. No significant difference was observed for those subpopulations between two groups (Figure 1A). These results suggest that iron overload does not influence the frequency of normal HSCs and HSC subpopulations in AML.

Next, we investigated whether iron overload had an impact on the proliferation and apoptosis of normal HSCs in AML. No significant difference was observed between MA9 and MA9/FE mice (Figures 1B, C). Colony forming ability determines the self-renewal potential of HSCs and partly reflects HSC function. MA9/FE HSCs formed significantly more BFU-E, CFU-GM and CFU-GEMM colonies than MA9 HSCs (Figure 1D, Supplementary Figure S2A). These results suggest that iron overload promotes the colony-forming capacity of normal HSCs in AML mice.

Iron overload skews myeloid differentiation of normal HSCs in AML mice

To determine whether iron overload affects differentiation of HSCs, the frequency of normal HPCs and more mature cells of multiple lineages in the BM of MA9 and MA9/FE mice was evaluated. CD34 and CD16/32 were used to identify the committed progenitor cells, $CD34^+$ $CD16/32^+$ GMP, $CD34^+$ $CD16/32^-$ CMP, and $CD34^-$ $CD16/32^-$ MEP were based on the $GFP^-Lin^-Sca1^-c\text{-}Kit^+$ population. A significant increase in the frequency of GMP was observed in MA9/FE mice when compared with that in MA9 mice (Figure 1E). In addition, iron overload resulted in a prominent increase in more mature compartments of myeloid cells, such as Mac-1^+, Gr-1^+ and F4/80^+ cells, in the BM (Figure 1F), suggesting that iron overload enhances myeloid lineage differentiation in AML.

Next, we performed a competitive repopulation assay to dissect the effect of iron overload on the hematopoietic reconstitution capacity of normal HSCs (Figure 1G). Donor-derived PB chimera rate of normal HSCs from MA9/FE mice was significantly higher than that from MA9 mice during the 16 weeks post-transplantation (Figure 1H, Supplementary Figure S2B). Moreover, similar results were also obtained for donor-derived BM chimera rate 16 weeks after transplantation (Figure 1I, Supplementary Figure S2C). These results indicate that iron overload promotes the hematopoietic reconstitution capacity of normal HSCs in AML. Though the donor-derived BM chimerism of HPCs populations, including CMP, GMP and MEP, showed no significant difference between MA9 and MA9/FE mice (Figure 1J, Supplementary Figure S2D), iron overload increased the donor-derived BM chimerism of myeloid lineages, including Gr-1^+ and F4/80^+ cells, while decreased the BM chimerism of $CD19^+$ B cells (Figure 1K). Together, these findings indicate that iron overload enhances the capacity of hematopoietic reconstitution and skews the myeloid differentiation of normal HSCs in AML.

More M2 macrophages correlates with a worse prognosis in iron overloaded AML patients

Ferritin consists of heavy and light chains, encoded by *FTH1* and *FTL* genes. CD68 and CD163 are typical markers for macrophages and M2 macrophages in humans. To assess the clinical significance of iron overload and macrophages in AML, the public TCGA database was used to analyze the expression levels of *FTH1*/*FTL* and *CD68*/*CD163* in leukemia patients and their correlations with disease prognosis. AML patients from TCGA datasets were divided into the $FTH1^{high}$, $FTH1^{low}$, FTL^{high}, and FTL^{low} groups, based on the median gene expression value of *FTH1* or *FTL*, respectively. $FTH1^{high}$ and FTL^{high} groups expressed higher level of CD68 or CD163 than their respectively counterparts, while $FTH1^{low}$ and FTL^{low} groups expressed lower level of CD68 or CD163 than their respectively counterparts (Figures 2A–D). We previously demonstrated that $FTH1^{high}$ group had a worse prognosis than $FTH1^{low}$ group (14). We further analyzed the overall survival (OS) of the $CD68^{high}$, $CD68^{low}$, $CD163^{high}$ and $CD163^{low}$ subgroups in the $FTH1^{high}$ or FTL^{high} groups. The results showed that no significant difference was detected between the $CD68^{high}$ and $CD68^{low}$ subgroups (Figures 2E, F) whereas the OS in the $CD163^{high}$ subgroup was significantly shorter than that in the $CD163^{low}$ subgroup (Figures 2G, H). The OS of the $CD68^{high}$, $CD68^{low}$, $CD163^{high}$ and $CD163^{low}$ subgroups in the $FTH1^{low}$ or FTL^{low} groups was also analyzed showing that no significant difference was detected between the $CD68^{high}$ and $CD68^{low}$ subgroups (Figures 2I, J), and between the $CD163^{high}$ and $CD163^{low}$ subgroup (Figures 2K, L). These results suggest that iron overload correlates with increased level of M2 macrophages and more M2 macrophages further correlates with a poor prognosis in iron overloaded AML patients.

Iron overload educates LAM with more M2 characteristics

The gene expression profile and activation phenotype of LAMs in the iron-overload AML microenvironment were studied. RNA-

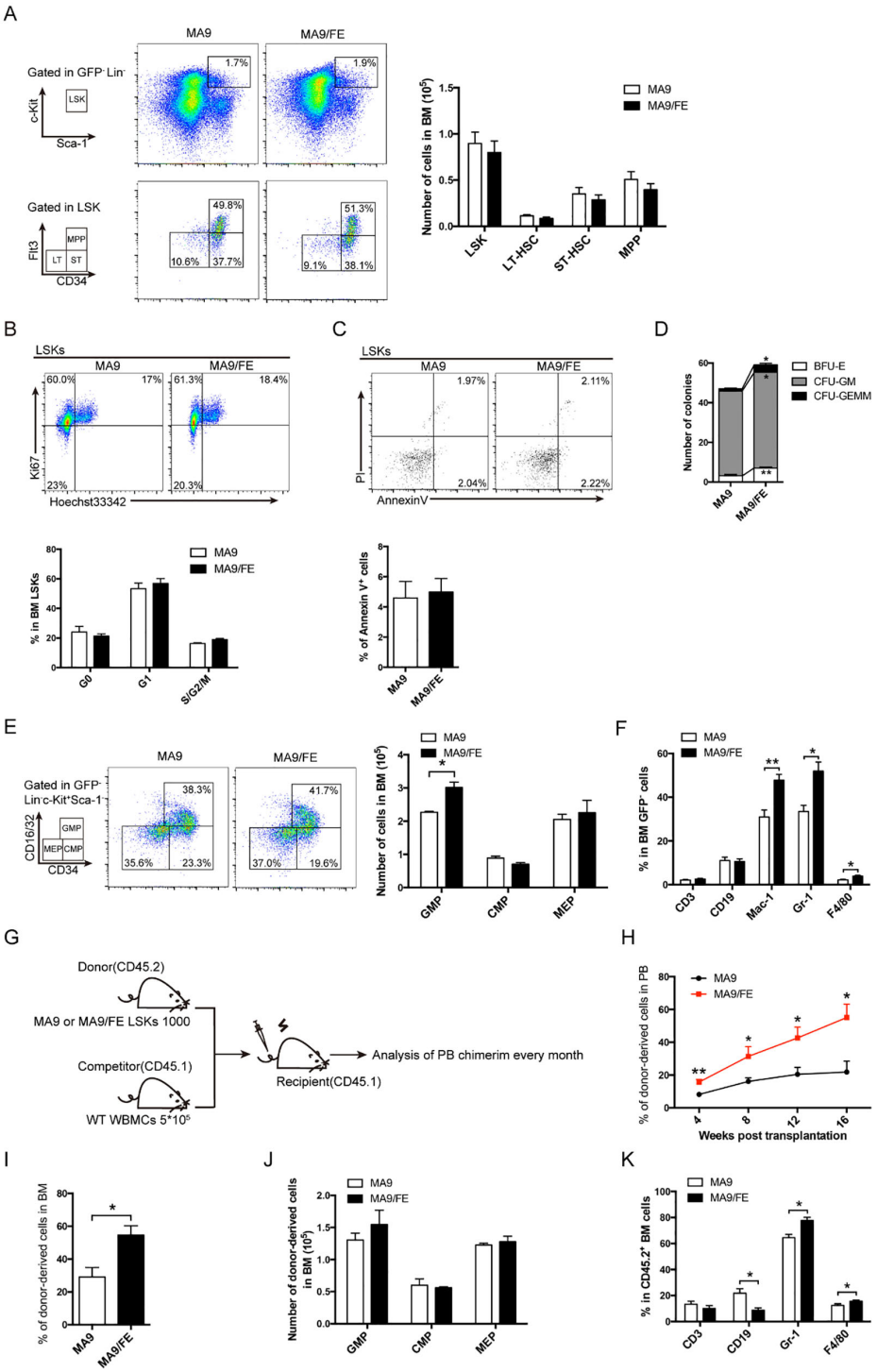

FIGURE 1
Normal HSPCs and more mature cells of multiple lineages in iron-overload AML mice. **(A)** Representative FACS plots and frequencies of normal HSC subpopulations (LSK: $Lin^{-}c\text{-}Kit^{+}Sca1^{+}$, LT-HSC: $CD34^{-}Flt3^{-}LSK^{+}$ ST-HSC: $CD34^{+}Flt3^{-}LSK^{+}$, MPP: $CD34^{+}Flt3^{+}LSK^{+}$) in the BM of MA9 and MA9/FE mice (n = 5). **(B)** Normal HSCs from the BM of MA9 and MA9/FE mice were stained with Ki67 and Hoechst 33342. The gating strategy for G0 (bottom left), G1 (top left), and S/G2/M (top right) is shown (top panel), and the percentage is plotted (n=5) (bottom panel). **(C)** Normal HSCs from the BM of MA9 and MA9/FE mice were stained with Annexin V and PI. The gating strategy for early (bottom right) and late (top right) phase apoptotic cells is shown (top panel), and the percentage of is plotted (n=5) (bottom panel). **(D)** Normal HSCs from the BM of MA9 or MA9/FE mice were seeded onto 24-well plates (500 cells/well) for colony forming assays, and the numbers of BFU-E, CFU-GM, and CFU-GEMM are plotted. **(E)** Representative FACS plots and frequencies of HPC subpopulations (GMP: $CD34^{+}CD16/32^{+}$, CMP: $CD34^{+}$ $CD16/32^{-}$, MEP: $CD34^{-}$ $CD16/32^{-}$, gated from $GFP^{-}Lin^{-}Sca1^{-}c\text{-}Kit^{+}$ population) in the BM of MA9 and MA9/FE mice (n = 5). **(F)** Lineage distribution in BM assessed by FACS (n = 5). **(G-K)** Competitive BM transplantation was performed and mice were sacrificed 16 weeks post-transplantation for chimerism analysis (n = 6). The schematic of the experiment design **(G)**, the chimerism of PB $CD45.2^{+}$ cells at indicated time points **(H)** as well as the chimerism of BM $CD45.2^{+}$ cells **(I)**, the absolute numbers of $CD45.2^{+}$ HPC populations **(J)** and the percentage of $CD45.2^{+}$ multiple lineages **(K)** are shown. The results are from three independent experiments. Unpaired Student's t test; $*p < 0.05$; $**p < 0.01$.

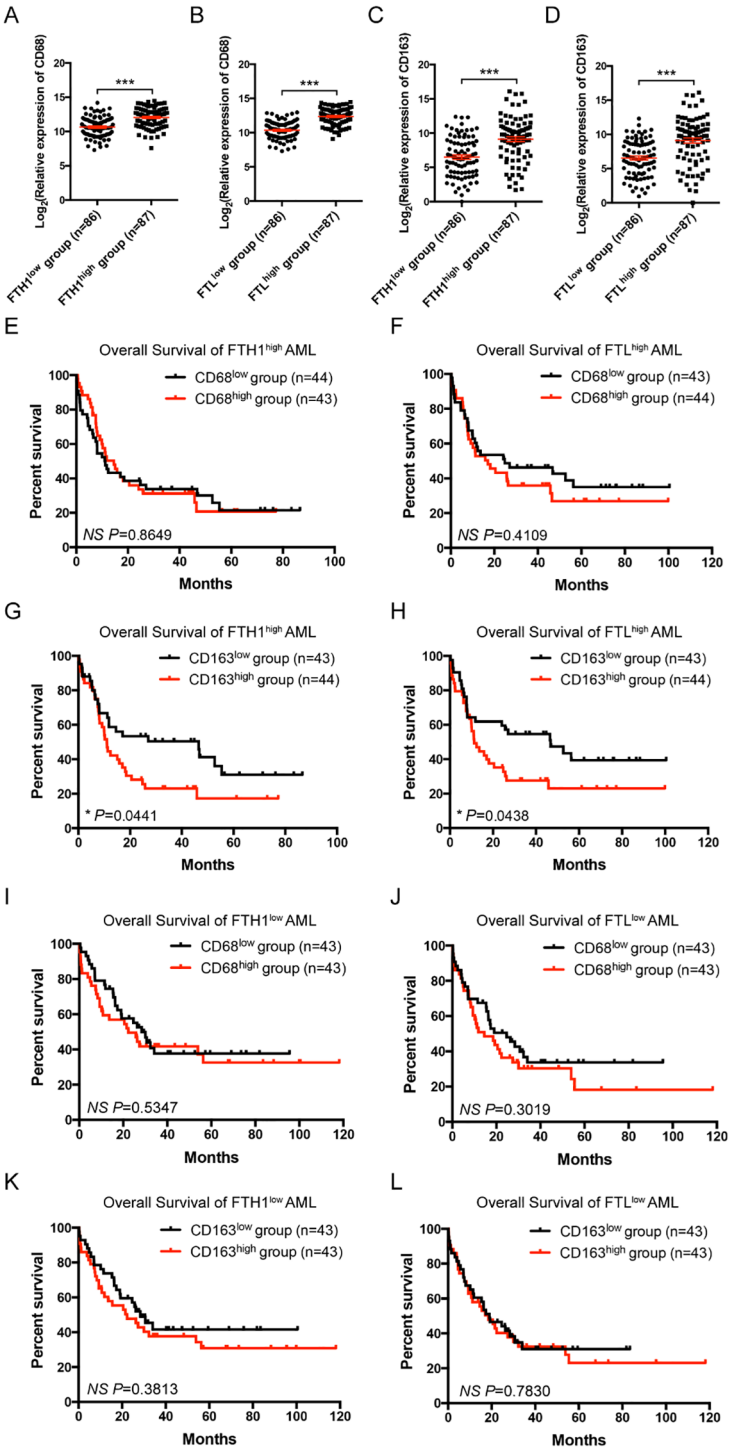

FIGURE 2
Correlation and clinical significance of ferritin and macrophage markers in AML patients. **(A-D)** Correlations between the relative expression of CD68 or CD163 and *FTH1* or *FTL* in TCGA are shown. AML cases were divided into the FTH1^{high}, FTH1^{low}, FTL^{high}, and FTL^{low} groups, based on the median gene expression value of *FTH1* or *FTL*, respectively, and the relative expression of CD68 **(A, B)** or CD163 **(C, D)** is plotted. **(E-H)** In the FTH1^{high} or FTL^{high} groups, AML cases were divided into CD68^{high}, CD68^{low}, CD163^{high}, and CD163^{low} subgroups, based on the median gene expression value of CD68 or CD163, respectively, and the OS of AML patients was compared by Kaplan-Meier analysis. **(I-L)** In the FTH1^{low} or FTL^{low} groups, AML cases were divided into CD68^{high}, CD68^{low}, CD163^{high}, and CD163^{low} subgroups, based on the median gene expression value of CD68 or CD163, respectively, and the OS of AML patients was compared by Kaplan-Meier analysis. Unpaired Student's t test; *$p < 0.05$; ***$p < 0.001$..

seq was performed to study gene expression profiles in the BM LAMs. Differentially expressed genes (DEGs) are plotted in Figure 3A (DEGs, FC ≥ 2, FDR ≤0.01), which reflect the modulatory effects of iron overload on LAM gene expression profile in leukemic microenvironment. A Venn diagram shows the numbers of DEGs between different pairs of samples (Supplementary Figure S3), and 29-shared DEGs are listed in Supplementary Table S3. Gene set enrichment analysis (GSEA) showed that the genes in the annotations, "myeloid leukocyte activation" and "macrophage activation", were enriched in MA9/FE LAMs versus WT/FE macrophages or MA9 LAMs (Figure 3B). To study the activation phenotype of MA9/FE LAMs, the dynamic expression of phenotype-associated genes (6 genes for M1 and 6 genes for M2) was monitored. The expression levels of M1- and M2-related genes (Figures 3C, D) showed considerable differences among different samples. To obtain an intuitive view of the phenotypes of macrophages from different samples, a two-dimensional illustration of macrophage phenotypes was used. When WT macrophages were used as control, WT/FE macrophages and MA9 LAMs were in the lower area, *i.e.* with more M1 characteristics, whereas MA9/FE LAMs were in the upper area, *i.e.* with more M2 characteristics (Figure 3E). Interestingly, iron overload educated WT macrophages towards M1 phenotype (WT/FE macrophages) whereas educated MA9 LAMs towards M2 phenotype (MA9/FE LAMs) (Figure 3E). These results suggest that LAMs show distinct transcriptional modulations in response to iron overload in the leukemic environment, and exhibit increased M2-related characteristics, potentially resulting in different biological activities and functions.

Iron overload decreases the phagocytic ability of LAMs

To evaluate the potential effects of iron overload on the functions of LAMs, DEG profiles were analyzed. GSEA showed that the genes in the annotations, "phagocytosis" and "phagocytosis engulfment", were enriched in MA9 LAMs versus WT controls, MA9/FE LAMs versus WT/FE controls, and MA9/FE LAMs versus MA9 LAMs (Figure 4A). Phagocytosis is an important functional characteristic of macrophages. Hence, non-specific, and specific phagocytosis were assessed. Non-specific phagocytosis was assessed using the latex bead uptake experiments. MA9 and MA9/FE LAMs had a decreased phagocytotic ability, when compared with their respective control macrophages (Figure 4B, Supplementary Figure S4A). Specific phagocytosis of AML cells was assessed using *in vitro* co-culture experiments. We found that in addition to the decreased phagocytotic ability of MA9 and MA9/FE LAMs, the phagocytotic ability of MA9/FE LAMs was much lower than that of MA9 LAMs (Figure 4C, Supplementary Figure S4B).

CD47/SIRPα axis is a major pathway in repressing the activation and phagocytosis of macrophages. Thus, CD47 expression on leukemia cells and SIRPα expression on LAMs were investigated. CD47 expression was upregulated in MA9/FE AML cells (Figure 4D), whereas no difference was observed in SIRPα expression between MA9 and MA9/FE LAMs (Figure 4E). These results demonstrate that LAMs have a low phagocytotic potential against AML cells in response to the iron overload in the leukemic microenvironment.

Iron overload promotes LAMs-mediated immunosuppression

GSEA results showed that the genes in the annotations, "activation of immune response" and "regulation of T cell activation", were enriched in MA9 LAMs versus WT controls, and MA9/FE LAMs versus WT/FE controls. Furthermore, the annotations, "cells activation involved in immune response" and "negative regulation of adaptive immune response", were enriched in MA9/FE LAMs versus MA9 LAMs (Figure 5A). Hence, the immunoregulatory potential of LAMs on T cells was analyzed using *in vitro* co-culture experiments. CD25 and CD44 expressions, which are generally related to T cell activation, were analyzed. A higher level of CD25 was detected in both $CD4^+$ and $CD8^+$ T cells co-cultured with MA9 or MA9/FE LAMs, than those co-cultured with their respective control macrophages. However, CD25 expression level decreased in $CD4^+$ and $CD8^+$ T cells co-cultured with MA9/FE LAMs, when compared with that with MA9 LAMs (Figures 5B–E). Furthermore, a higher level of CD44 was detected in $CD4^+$ T cells co-cultured with MA9 or MA9/FE LAMs, than those co-cultured with their control macrophages. However, CD44 expression level decreased in $CD4^+$ and $CD8^+$ T cells co-cultured with MA9/FE LAMs, when compared with that with MA9 LAMs (Figures 5F–I). These results suggest that iron overload induces the inhibition of LAMs-mediated T cell activation.

Iron overload promotes LAMs to acquire tolerogenic phenotypes that may contribute to T cell exhaustion

To further evaluate the potential mechanism of LAMs-induced immune dysfunction in iron-overload leukemic microenvironment, the expression of immune checkpoints on LAMs was detected. No difference was observed in the expression levels of PD-L1, CD200 and Galectin9, the immune checkpoint ligands, between MA9 LAMs and their control macrophages. However, MA9/FE LAMs expressed higher levels of these molecules than those on control macrophages or MA9 LAMs (Figures 6A–F).

Next, the expression levels of PD-1, CD200R and Tim3, the immune checkpoint receptors, on T cells after *in vitro* co-cultured with macrophages were detected. $CD4^+$ T cells co-cultured with MA9 or MA9/FE LAMs expressed higher level of PD-1 than those co-cultured with control macrophages. $CD4^+$ T cells co-cultured with MA9/FE LAMs expressed higher levels of CD200R and Tim3 than those co-cultured with control macrophages. Furthermore, $CD4^+$ T cells co-cultured with MA9/FE LAMs had higher expression levels of CD200R and Tim3 than those co-cultured with MA9 LAMs (Figure 6G, Supplementary Figures S5A–C).

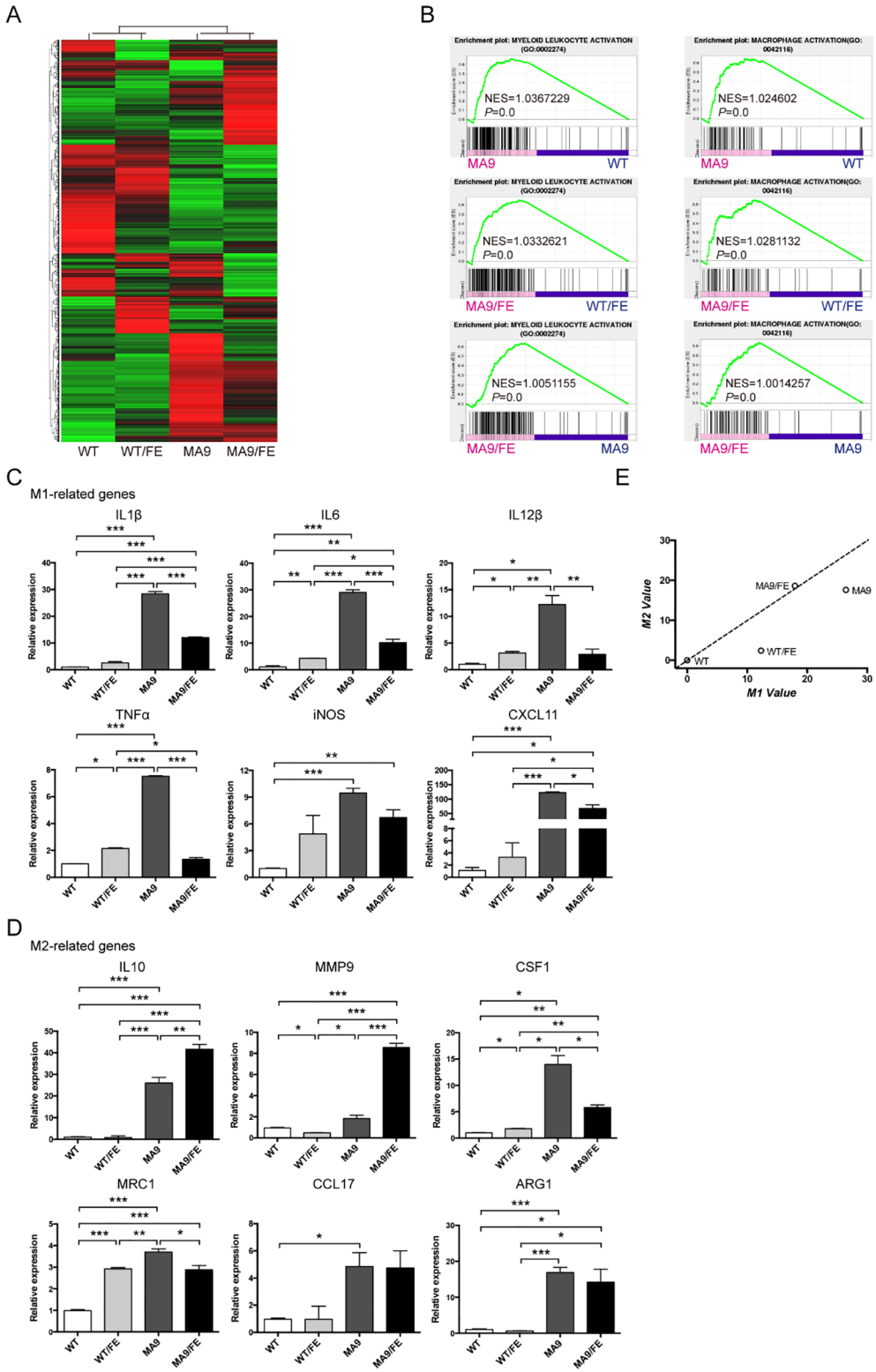

FIGURE 3
Iron overload affects the gene expression profile and activation phenotype of LAMs. Macrophages were sorted from the BM of MA9, MA9/FE mice and their respective normal counterparts (WT and WT/FE mice), and RNA-seq was performed. **(A)** DEG (FC ≥ 2, FDR ≤ 0.01) expression profiles are shown. **(B)** GSEA shows the enrichment of genes in annotations between MA9/FE LAMs and WT/FE macrophages or MA9 LAMs. Expression of M1 **(C)** and M2 **(D)** phenotype-associated genes in macrophages was detected by real-time PCR. For each gene, the RQ value of WT macrophages was designated 1.000, respectively. **(E)** A two-dimensional illustration of the macrophage phenotype is shown. For each gene, the value of the WT macrophages was designated 0. The mean values of the relative expression of genes mentioned above were used for the calculation and the M1 and M2 values. The results are from three independent experiments. Unpaired Student's t test; *$p < 0.05$; **$p < 0.01$; ***$p < 0.001$..

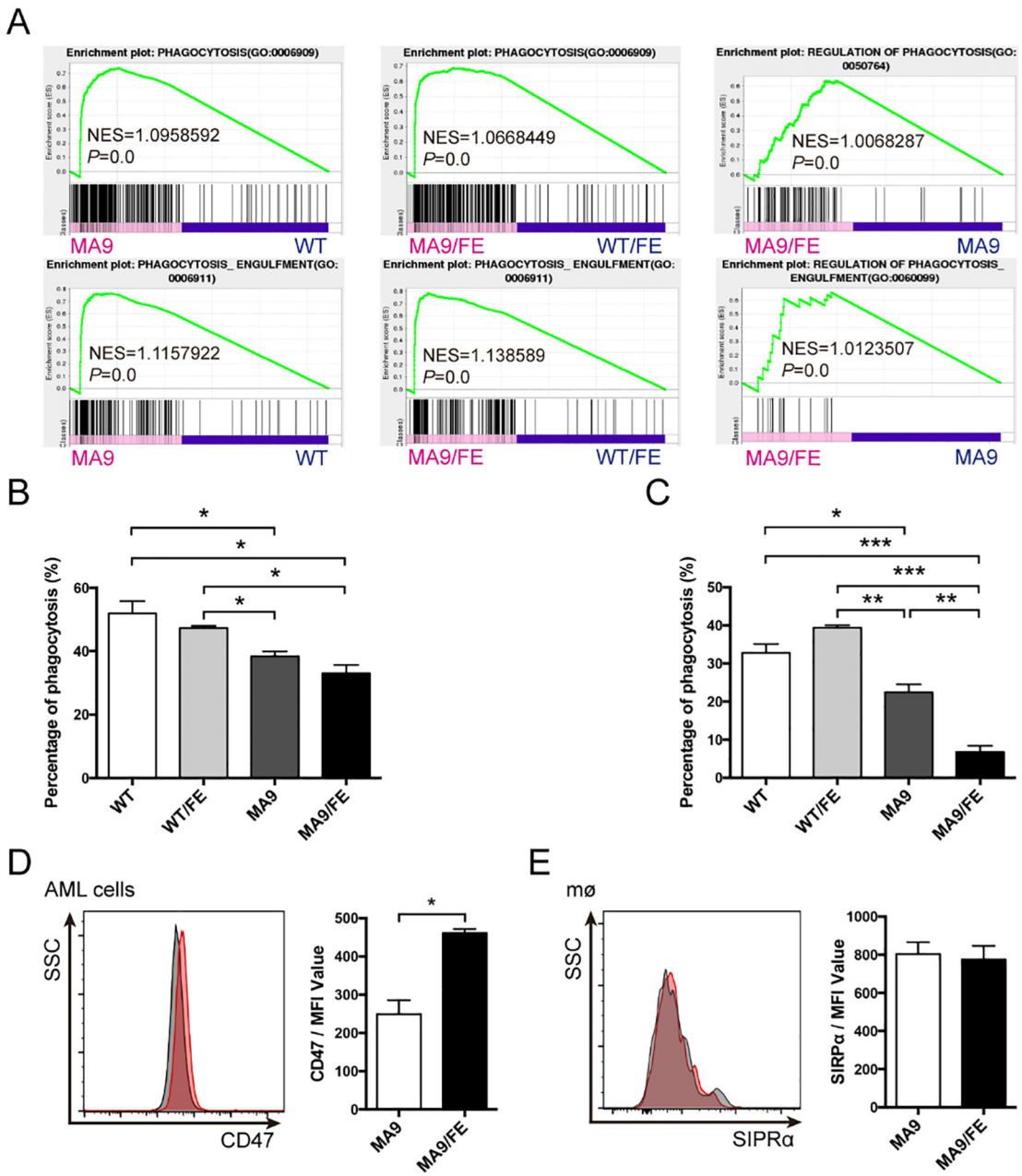

FIGURE 4
Iron overload decreases the phagocytic ability of LAMs. **(A)** GSEA shows the enrichment of genes in annotations between MA9/FE LAMs and WT/FE macrophages or MA9 LAMs. **(B)** Macrophages sorted from the BM of WT, WT/FE, MA9 or MA9/FE mice were cultured with FITC-labeled 2 μm latex beads for 15 mins, and the phagocytic activity was assessed by FACS (n=5). **(C)** Macrophages sorted from the BM of WT, WT/FE, MA9 or MA9/FE mice were cocultured with sorted leukemia cells for 18 hrs. Cells were collected, and the proportion of GFP^+ cells was analyzed by FACS (n=5). AML cells cultured alone were used as a blank control. The phagocytotic rate was calculated as follows: (100%- 18 hrs (test))-(100%- blank control). **(D, E)** The expressions of CD47 on leukemia cells **(D)** and SIRPα on LAMs **(E)** were detected by FACS. The results are from three independent experiments. Unpaired Student's t test; *$p < 0.05$; **$p < 0.01$; ***$p < 0.001$.

$CD8^+$ T cells co-cultured with MA9/FE LAMs expressed higher levels of PD-1 and CD200R than those co-cultured with control macrophages. Additionally, $CD8^+$ T cells co-cultured with MA9/FE LAMs had higher expression levels of PD-1 and CD200R than those co-cultured with MA9 LAMs (Figure 6H, Supplementary Figures S5D–F). These results suggest that iron overload promotes LAMs acquisition of tolerogenic phenotypes that may contribute to T cell exhaustion.

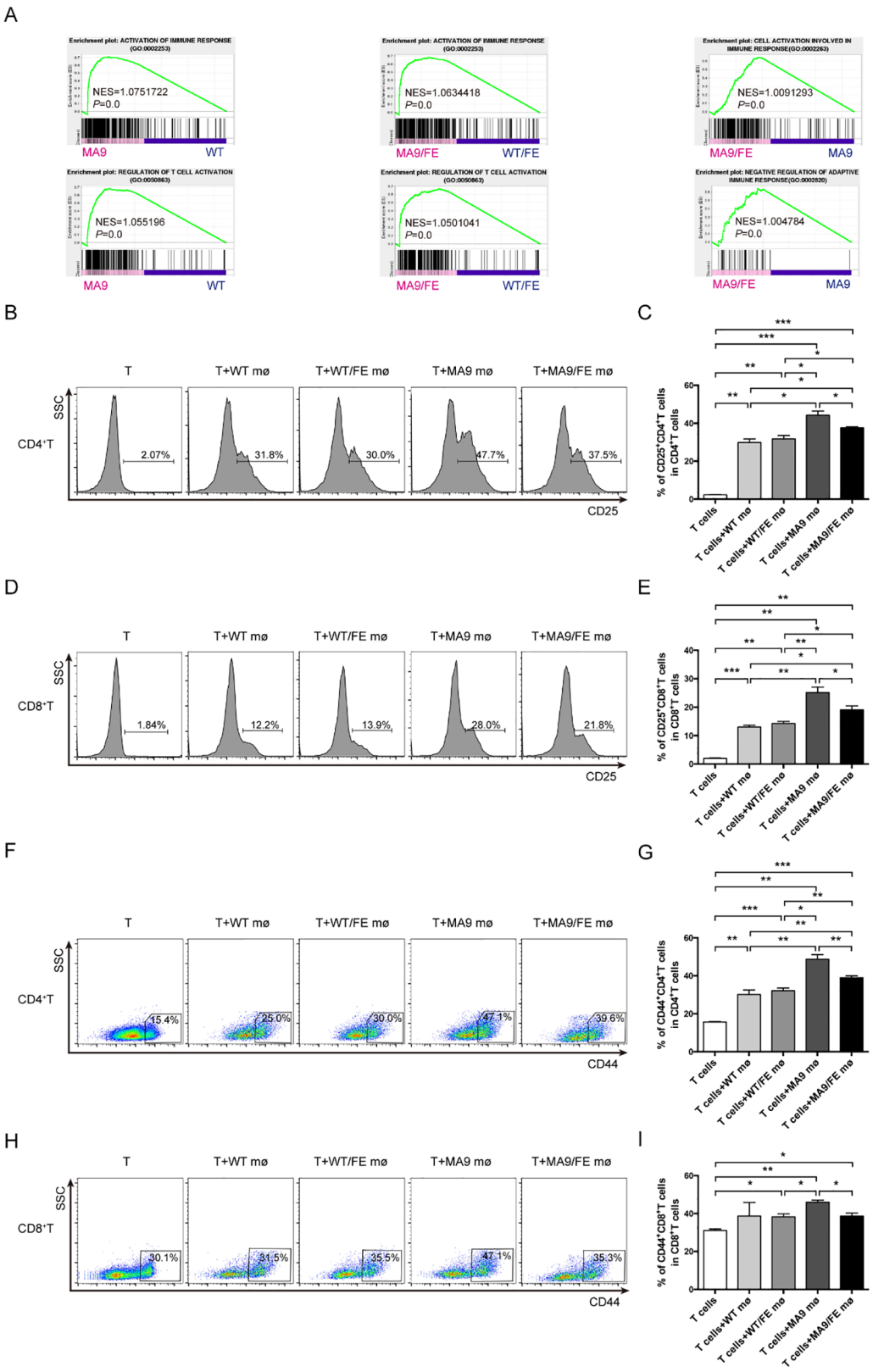

FIGURE 5
Iron overload promotes LAMs-mediated T cell activation inhibition. **(A)** GSEA shows the enrichment of genes in annotations between MA9/FE LAMs and WT/FE macrophages or MA9 LAMs. **(B-I)** Freshly sorted T cells from the spleen of WT mice were cocultured with macrophages from the BM of WT, WT/FE, MA9 or MA9/FE mice in 48-well plates for 48 hrs (n=5). T cells cultured without macrophages were set as the blank group. Typical FACS results **(B)** and the expression of CD25 in $CD4^+$ T cells **(C)** are shown. Typical FACS results **(D)** and the expression of CD25 in $CD8^+$ T cells **(E)** are shown. Typical FACS results **(F)** and the expression of CD44 in $CD4^+$ T cells **(G)** are shown. Typical FACS results **(H)** and the expression of CD44 in $CD8^+$ T cells **(I)** are shown. The results are from three independent experiments. Unpaired Student's t test; *$p < 0.05$; **$p < 0.01$; ***$p < 0.001$.

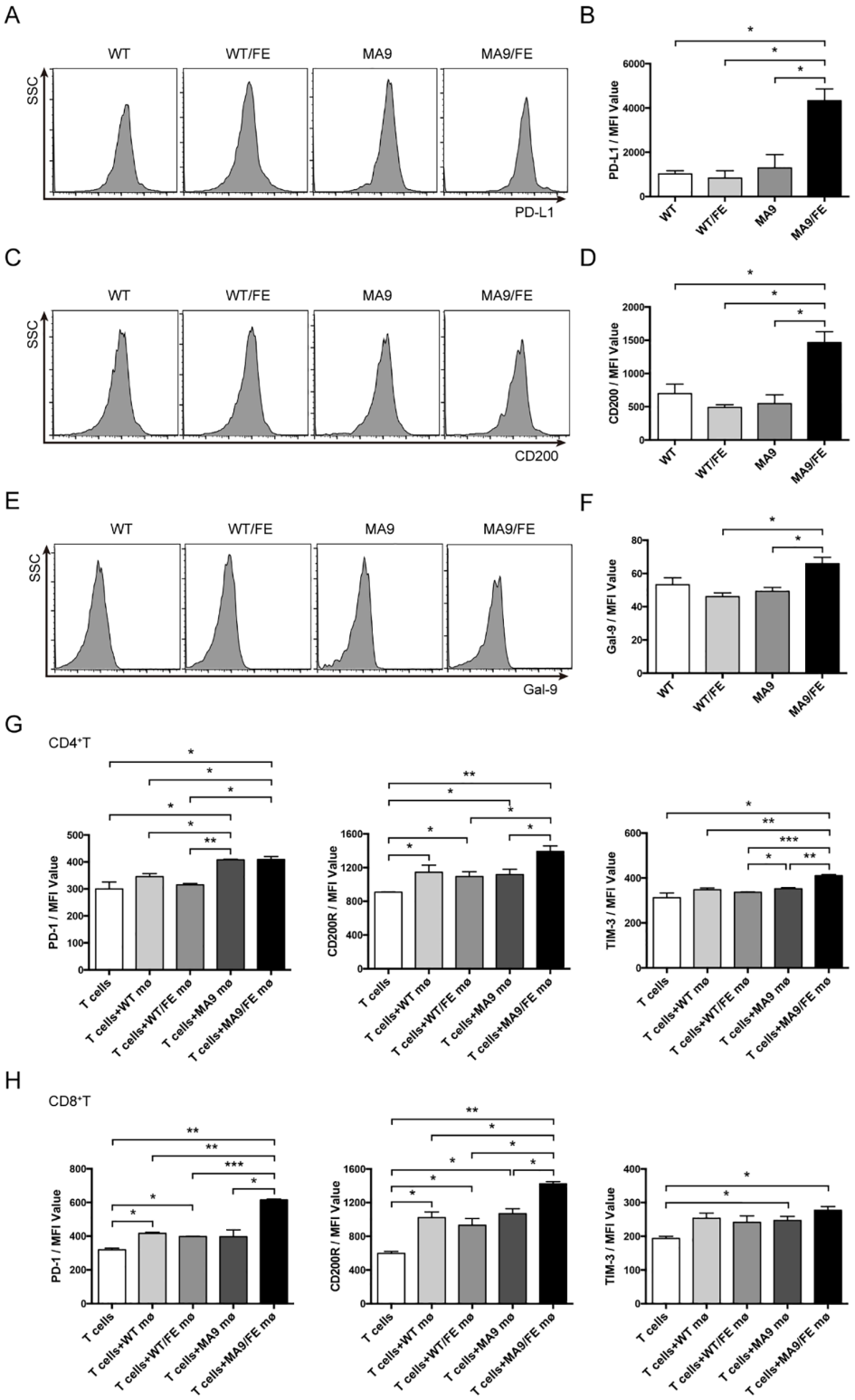

FIGURE 6
Iron overload promotes LAMs-mediated T cell exhaustion. Macrophages from the BM of WT, WT/FE, MA9 or MA9/FE mice were sorted, and the expression of immune checkpoint genes was analyzed. Typical FACS results **(A)** and the expression of PD-L1 in BM macrophages in MFI **(B)** are shown. Typical FACS results **(C)** and the expression of CD200 in BM macrophages in MFI **(D)** are shown. Typical FACS results **(E)** and the expression of Gal-9 in BM macrophages in MFI **(F)** are shown. **(G, H)** Freshly sorted T cells from the spleen of WT mice were cocultured with macrophages from the BM of WT, WT/FE, MA9 or MA9/FE mice in 48-well plates for 48 hrs (n=5). T cells cultured without macrophages were set as the blank group. The expressions of PD-1, CD200R and TIM-3 in $CD4^+$ **(G)** or $CD8^+$ **(H)** T cells were detected by FACS and are shown in MFI. The results are from three independent experiments. Unpaired Student's t test; *$p < 0.05$; **$p < 0.01$; ***$p < 0.001$.

Iron overload accelerates AML progression and depletion of LAMs hinders AML progression

Given the suppressive phagocytic function of LAMs and LAM-induced immune dysfunction in response to iron overload, we investigated whether *in vivo* LAM depletion alters the effects of iron overload on AML progression (Figure 7A). MA9/FE mice had a significantly shorter survival time than MA9 mice. Although it could not prolong the survival of either MA9 or MA9/FE mice (Figure 7B), LAM depletion by liposomal clodronate significantly decreased PB leukemia cell levels in both MA9 and MA9/FE mice on day 26 (Figure 7C). Tissue sections from leukemic mice were subjected to H&E staining showing that leukemia cell-infiltrating areas in tissues, including the BM, liver, and spleen, were significantly larger in MA9/FE mice than those in MA9 mice (Figure 7D). The infiltration of leukemia cells in the pulmonary veins was more severe in MA9/FE mice than that in MA9 mice. Additionally, a massive aggregation of leukemia cells was detected in the renal pelvis in MA9/FE mice. However, the depletion of LAMs decreased the infiltration of leukemia cells in tissues, including the BM, liver, spleen, lung and kidneys, in both MA9 and MA9/FE mice. Collectively, these findings indicate that iron overload shortens the survival time of AML mice, whereas the depletion of LAMs in iron-overload microenvironment hinders AML development.

Discussion

In hematological malignancies, although iron overload in AML is not as common as in MDS, systemic iron overload is still a big clinical challenge as the results of ineffective hematopoiesis and disease-specific therapies. The increased iron level correlates with a poorer overall survival rate, a higher incidence of relapse and a suppressed autologous stem cell mobilization in AML patients (11, 12, 40). Nevertheless, the pathological significance of iron overload in AML has not received sufficient attention, and its pathological roles and mechanisms have not been elucidated. So, it is necessary to explore. The hematopoietic ecosystem comprises all cellular and non-cellular component of the hematopoietic system (41). Iron overload modifies the hematopoietic ecosystem to exert influence on normal or disease hematopoiesis. We previously dissected the direct effects of iron overload on leukemia cells (14). Here, we try to understand the indirect effects of iron overload on leukemia progression, *i.e.* the changes in other components of the hematopoietic ecosystem, specifically HSCs and LAMs. The results will give deeper understanding of the pathologic mechanisms of iron overload in leukemia.

HSCs not only maintain the decreased production of normal blood cells in leukemia, but also determine the effective recovery from the disease. Evidence has shown the progressively suppressed function of normal HSPCs in the impaired normal hematopoietic niche during leukemogenesis (17, 18, 28, 29). Furthermore, an intricate interplay between iron and HSCs has been revealed for HSC maintenance and fate decision (21, 22, 24, 42, 43). Both iron overload and iron deficiency disrupt HSC homeostasis, highlighting the delicate balance required for optimal hematopoietic function. Here, we report that iron overload did not further impact HSC maintenance in AML, which was distinct from those iron-induced changes in HSCs under steady state and stress conditions (21, 42, 43). This difference may due to the complexity of the disease-specific microenvironment. However, iron overload promoted the colony-forming capacity and further skewed myeloid differentiation of HSCs in AML. The myeloid-biased differentiation is one of the characteristics of senescent HSC (44, 45). HSC senescence affects the progression of leukemia, and is considered as a main factor resulting in the high incidence of AML in the elderly, which has important clinical implications. Intrinsic and extrinsic factors have been implicated in driving HSC senescence, such as DNA damage and mitochondrial damage, *etc.* (46, 47), which are also regulated by iron (48). Thus, iron overload may be involved in HSC senescence and play adverse roles in leukemia progression.

Different immune cells form the immunomicroenvironment in the hematopoietic ecosystem. They play sophisticated roles in leukemia (25, 28, 29, 49). Among them, macrophages attract much attention (50, 51). Although the M1 (classically activated macrophage) and M2 (alternatively activated macrophage) binary classification of macrophage activation phenotypes is well accepted (52), macrophage activation is more complex as they are signal-dependently activated into a continuum of states between the two extremes (31, 32). We previously found LAMs were educated by the leukemic microenvironment to exhibit unique phenotypes and functions (30–32). Recent studies suggested that iron metabolism was involved in regulating macrophage polarization (53), and induced tremendous plasticity of either M1- or M2- like phenotype under distinct conditions (33–38). These seemingly contradictory results highlight a context- dependent macrophage polarization. Here, we established a connection between iron metabolism and macrophage in AML. Iron overload correlates with increased M2 macrophages, which further correlate with a poor prognosis in iron overloaded AML patients. As the major iron storage protein, ferritin consists of the heavy and light chains, encoded by FTH1 and FTL genes. Using the expression level of FTH1 and FTL to reflect iron overload is not a specific indicator for iron overload in leukemia and has limitation. However, due to convenient sample collection and relatively low testing cost, ferritin is still considered as the preferred method for diagnosing iron overload in clinical practice. Dynamic monitoring the serum ferritin level in a cohort can more accurately determine iron overload status and give more solid conclusion. Nevertheless, analysis of transcriptional levels of FTH1 and FTL genes from public databases can also give clues for the correlation between macrophage activation and prognosis in iron overloaded AML patients. Using CD68 and CD163 to define macrophages and M2 macrophages in human is simple but has obvious limitations. Despite the fact that M2 macrophages have great heterogeneity and there is no well-accepted transcriptional profile to define M2 macrophages, using multiple genes or even whole genome transcriptional profile will improve the performance. The

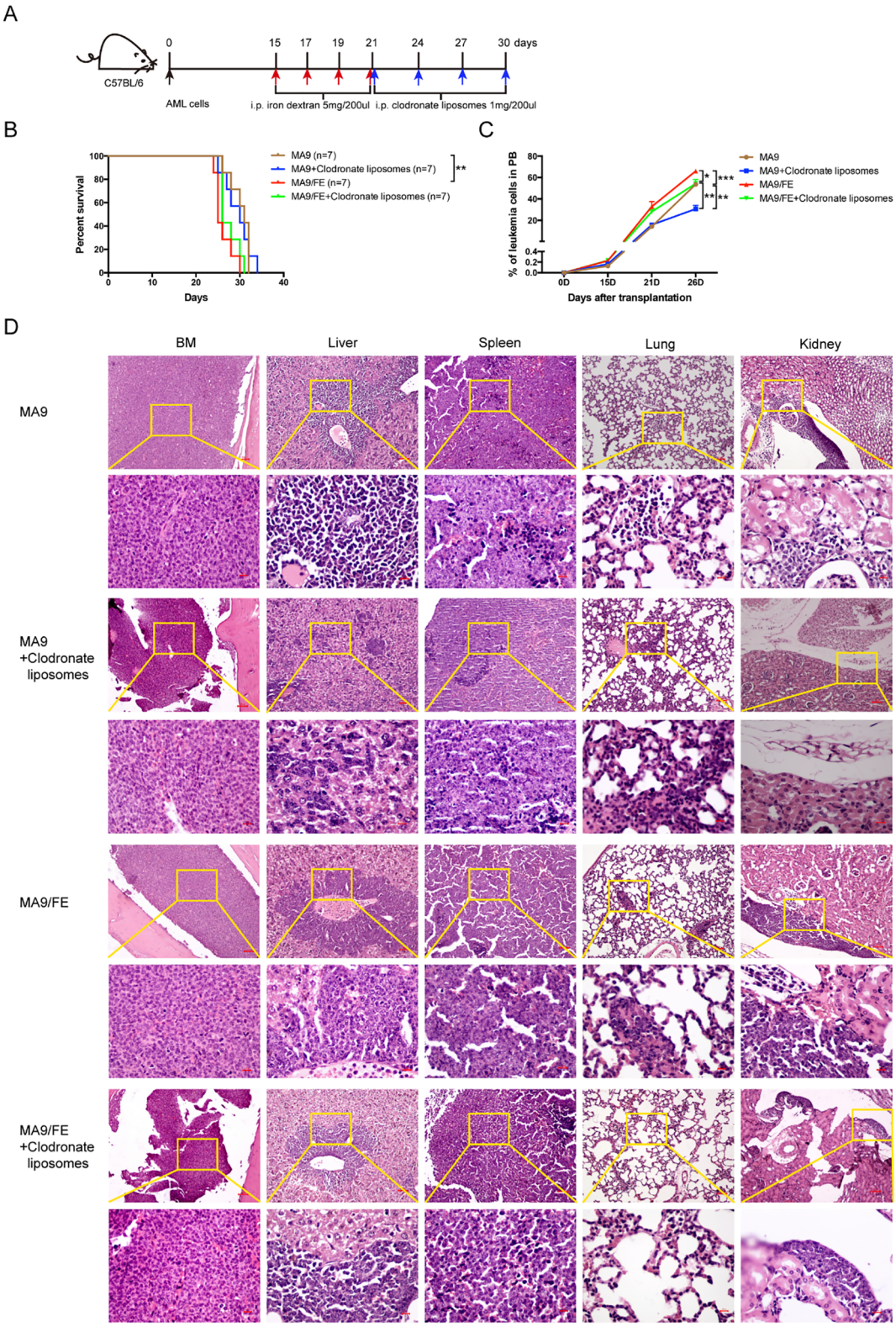

FIGURE 7
Depletion of LAMs hinders iron overload caused acceleration of AML progression. **(A)** Schematic of the experiment design is shown. **(B)** The mouse survival time was recorded, and Kaplan–Meier analysis was performed (n = 7). **(C)** PB leukemia cells were monitored at the indicated time points during the progression of leukemia. **(D)** Typical H&E-stained sections of BM, liver, spleen, lung, and kidney are shown. Scale bars (100 μm or 50 μm) are indicated. The results are from three independent experiments. Unpaired Student's t test; *$p < 0.05$; **$p < 0.01$; ***$p < 0.001$.

approaches like CIBERSORT-based immune de-convolution may give better results. However, due to the simplicity and convenience during the detection process at any time, using a typical marker to define macrophages is still a well-adopted method in the literature. Furthermore, we demonstrated a phenotypic shift, i.e. iron overload educated LAMs to exhibit more M2 characteristics. It's well accepted that M1 or M1-like macrophages have anti-tumoral functions while M2 or M2-like macrophages are pro-tumoral (54). Therefore, overloaded iron may further educate LAMs to have more pro-leukemic effects.

Phagocytosis is an important functional characteristic of macrophages. It's an effective strategy in cancer immunotherapy to potentiate macrophages for phagocytosis. We observed that iron overload decreased the phagocytic potential of LAMs, suggesting a decreased anti-leukemic effect. CD47/SIRPα axis is a major pathway in repressing the phagocytic function of macrophages (55, 56). CD47 was upregulated in iron-overload AML cells, which was consistent with the results in hMRP8bcr/abl × hMRP8bcl2 leukemic cells (57). By contrast, no difference was detected in the expression of SIRPα between MA9 and MA9/FE LAMs. Therefore, iron overload further inhibited the phagocytosis of LAMs against leukemia cells. These events may at least partly account for the accelerated AML progression mediated by iron overload.

Macrophages are an essential regulator of the intricate immune regulatory network in disease microenvironments. AML associated immune dysfunction is also mediated by T cells with impaired phenotypes (58–61), which is considered to be directly induced by malignant cells. However, we previously suggested the crosstalk between LAMs and T cells, and proved that LAMs directly regulated T cell activation (31). Here, we further demonstrated that iron overload promoted LAMs-mediated immunosuppression on T cells in several ways. On the one hand, the decreased CXCL11 level, a potent chemoattractant for T cells acting (62), expressed by LAMs in iron-overload mice, may contribute to fewer effector T cells in AML. On the other hand, iron overload induced the skewing of LAMs toward a tolerogenic phenotype with aberrant immune checkpoint expressions, which may contribute to T cell exhaustion leading to immune escape and progression acceleration in AML. Hence, due to the defective phenotype and suppressed functions of LAMs caused by iron overload, we postulated that LAM depletion might decrease the effects of iron overload on AML. Successfully, LAM depletion by liposomal clodronate attenuated iron overload-mediated acceleration of AML progression. In line with this result, macrophage depletion also delayed chronic lymphocytic leukemia development (63). Hence, our data emphasize that *in vivo* manipulation of macrophages has a pronounced impact on iron overloaded AML progression and suggest that AML should be an excellent candidate for cancer immunotherapy.

Taken together, we demonstrate that iron overload has a significant impact on normal HSCs and LAMs in the leukemic hematopoietic ecosystem, which contribute to the adverse roles of iron overload in AML progression. Therefore, we identify that the overloaded iron is a vital factor driving remodeling the BM microenvironment in AML. These findings provide new insights into the pathophysiologic mechanisms of iron overload in AML and broaden the knowledge of multifaceted roles of iron overload in malignancies.

Data availability statement

The datasets presented in this study can be found in online repositories. The names of the repository/repositories and accession number(s) can be found in the article/Supplementary Material.

Ethics statement

The animal study was approved by Animal Care Committee of the Institute of Hematology and Blood Diseases Hospital, CAMS & PUMC. The study was conducted in accordance with the local legislation and institutional requirements.

Author contributions

FY: Conceptualization, Data curation, Formal analysis, Funding acquisition, Investigation, Validation, Visualization, Writing – original draft, Writing – review & editing. SL: Formal analysis, Investigation, Writing – review & editing. DY: Formal analysis, Investigation, Writing – review & editing. XC: Data curation, Formal analysis, Validation, Writing – review & editing. DZ: Data curation, Formal analysis, Validation, Writing – review & editing. HW: Formal analysis, Validation, Writing – review & editing. YL: Formal analysis, Investigation, Validation, Writing – review & editing. WX: Formal analysis, Investigation, Validation, Writing – review & editing. LW: Project administration, Supervision, Writing – review & editing. XiZ: Project administration, Supervision, Writing – review & editing. GZ: Conceptualization, Supervision, Validation, Visualization, Writing – review & editing. XuZ: Conceptualization, Supervision, Writing – review & editing.

Funding

The author(s) declare financial support was received for the research and/or publication of this article. The work was supported by grant 82000160 from the National Natural Science Foundation of China (NSFC); and grant YKK21138 from the Nanjing Municipal Health Science and Technology Development Project.

Acknowledgments

The authors greatly acknowledge the assistance of Animal Care Committee of the Institute of Hematology and Blood Diseases Hospital, CAMS & PUMC for animal care.

Conflict of interest

The authors declare that the research was conducted in the absence of any commercial or financial relationships that could be construed as a potential conflict of interest.

Generative AI statement

The author(s) declare that no Generative AI was used in the creation of this manuscript.

Publisher's note

All claims expressed in this article are solely those of the authors and do not necessarily represent those of their affiliated organizations, or those of the publisher, the editors and the reviewers. Any product that may be evaluated in this article, or claim that may be made by its manufacturer, is not guaranteed or endorsed by the publisher.

Supplementary material

The Supplementary Material for this article can be found online at: https://www.frontiersin.org/articles/10.3389/fimmu.2025.1626888/full#supplementary-material

SUPPLEMENTARY FIGURE 1
Iron overload validation in iron overloaded MLL-AF9-induced AML mouse model. Perl's iron staining of the BM, liver, spleen, heart, lung, and kidney. Scale bars (100 μm) are indicated. The results are from three independent experiments.

SUPPLEMENTARY FIGURE 2
Representative morphological characteristics of the HSC colony types and gating strategy for donor-derived CD45.2$^+$ cells in the PB and BM of recipients. **(A)** Typical BFU-E, CFU-GM, and CFU-GEMM colonies observed in this study are shown. **(B)** Representative FACS plots show the chimerism of donor-derived CD45.2$^+$ in the PB of recipients during 16 weeks post-transplantation (n = 6). **(C)** Representative FACS plots show the chimerism of donor-derived CD45.2$^+$ in the BM of recipients at 16 weeks post-transplantation (n = 6). **(D)** Representative FACS plots show the chimerism of donor-derived CD45.2$^+$ HPC subpopulations (GMP: CD34$^+$CD16/32$^+$, CMP: CD34$^+$ CD16/32$^-$, MEP: CD34$^-$CD16/32$^-$, based on CD45.2$^+$ Lin$^-$Sca1$^-$ c-Kit$^+$ population) in the BM of recipients at 16 weeks post-transplantation (n = 6). The results are from three independent experiments.

SUPPLEMENTARY FIGURE 3
Venn diagram of DEGs from different pairs of macrophages. Macrophages were sorted from the BM of MA9, MA9/FE mice and their respective normal counterparts (WT and WT/FE mice), and RNA-seq was performed. Venn diagram shows overlaps of the DEGs obtained from different pairs of macrophages.

SUPPLEMENTARY FIGURE 4
Typical FACS results of experiments testing the non-specific and specific phagocytic activity of macrophages. **(A)** Representative FACS plots show the non-specific phagocytic activity of macrophages. **(B)** Representative FACS plots show the lived AML cells cultured with or without macrophages. The results are from three independent experiments.

SUPPLEMENTARY FIGURE 5
Typical FACS results of immune checkpoint genes expressed on T cells cocultured with macrophages. Freshly sorted T cells from the spleen of WT mice were cocultured with macrophages from the BM of WT, WT/FE, MA9 or MA9/FE mice in 48-well plates for 48 hrs. T cells cultured without macrophages were set as the blank control. Expressions of PD-1, CD200R and TIM-3 in CD4$^+$ **(A-C)** or CD8$^+$ **(D-F)** T cells were detected by FACS. The results are from three independent experiments.

References

1. Möller HE, Bossoni L, Connor JR, Crichton RR, Does MD, Ward RJ, et al. Iron, myelin, and the brain: neuroimaging meets neurobiology. *Trends Neurosci*. (2019) 42:384–401. doi: 10.1016/j.tins.2019.03.009

2. Gao H, Jin Z, Bandyopadhyay G, Wang G, Zhang D, Rocha KCE, et al. Aberrant iron distribution via hepatocyte-stellate cell axis drives liver lipogenesis and fibrosis. *Cell Metab*. (2022) 34:1201–1213. doi: 10.1016/j.cmet.2022.07.006

3. Rhee J-W, Yi H, Thomas D, Lam CK, Belbachir N, Tian L, et al. Modeling secondary iron overload cardiomyopathy with human induced pluripotent stem cell-derived cardiomyocytes. *Cell Rep*. (2020) 32:107886. doi: 10.1016/j.celrep.2020.107886

4. Roemhild K, von Maltzahn F, Weiskirchen R, Knüchel R, von Stillfried S, Lammers T. Iron metabolism: pathophysiology and pharmacology. *Trends Pharmacol Sci*. (2021) 42:640–56. doi: 10.1016/j.tips.2021.05.001

5. Koleini N, Shapiro JS, Geier J, Ardehali H. Ironing out mechanisms of iron homeostasis and disorders of iron deficiency. *J Clin Invest*. (2021) 131:e148671. doi: 10.1172/JCI148671

6. Franke G-N, Kubasch AS, Cross M, Vucinic V, Platzbecker U. Iron overload and its impact on outcome of patients with hematological diseases. *Mol aspects Med*. (2020) 75:100868. doi: 10.1016/j.mam.2020.100868

7. Döhner H, Weisdorf DJ, Bloomfield CD. Acute myeloid leukemia. *New Engl J Med*. (2015) 373:1136–52. doi: 10.1056/NEJMra1406184

8. Newell LF, Cook RJ. Advances in acute myeloid leukemia. *BMJ*. (2021) 375:n2026. doi: 10.1136/bmj.n2026

9. Aifantis I, Raetz E, Buonamici S. Molecular pathogenesis of T-cell leukaemia and lymphoma. *Nat Rev Immunol*. (2008) 8:380–90. doi: 10.1038/nri2304

10. Lyons RM, Marek BJ, Paley C, Esposito J, McNamara K, Richards PD, et al. Relation between chelation and clinical outcomes in lower-risk patients with myelodysplastic syndromes: Registry analysis at 5 years. *Leukemia Res*. (2017) 56:88–95. doi: 10.1016/j.leukres.2017.01.033

11. Wermke M, Eckoldt J, Götze KS, Klein SA, Bug G, de Wreede LC, et al. Enhanced labile plasma iron and outcome in acute myeloid leukaemia and myelodysplastic syndrome after allogeneic haemopoietic cell transplantation (ALLIVE): a prospective, multicentre, observational trial. *Lancet Haematol*. (2018) 5: e201–e10. doi: 10.1016/S2352-3026(18)30036-X

12. Bertoli S, Paubelle E, Bérard E, Saland E, Thomas X, Tavitian S, et al. Ferritin heavy/light chain (FTH1/FTL) expression, serum ferritin levels, and their functional as well as prognostic roles in acute myeloid leukemia. *Eur J Haematol*. (2019) 102:131–42. doi: 10.1111/ejh.13183

13. Alva LC, Bacher U, Seipel K, Mansouri Taleghani B, Mueller BU, Novak U, et al. Iron overload is correlated with impaired autologous stem cell mobilization and survival in acute myeloid leukemia. *Transfusion*. (2018) 58:2365–73. doi: 10.1111/trf.14895

14. Yang F, Cui X, Wang H, Zhang D, Luo S, Li Y, et al. Iron overload promotes the progression of MLL-AF9 induced acute myeloid leukemia by upregulation of FOS. *Cancer letters*. (2024) 583:216652. doi: 10.1016/j.canlet.2024.216652

15. Joshi SK, Nechiporuk T, Bottomly D, Piehowski PD, Reisz JA, Pittsenbarger J, et al. The AML microenvironment catalyzes a stepwise evolution to gilteritinib resistance. *Cancer Cell*. (2021) 39:999–1014. doi: 10.1016/j.ccell.2021.06.003

16. Duarte D, Hawkins ED, Lo Celso C. The interplay of leukemia cells and the bone marrow microenvironment. *Blood*. (2018) 131:1507–11. doi: 10.1182/blood-2017-12-784132

17. Cheng H, Hao S, Liu Y, Pang Y, Ma S, Dong F, et al. Leukemic marrow infiltration reveals a novel role for Egr3 as a potent inhibitor of normal hematopoietic stem cell proliferation. *Blood*. (2015) 126:1302–13. doi: 10.1182/blood-2015-01-623645

18. Hu X, Shen H, Tian C, Yu H, Zheng G, XuFeng R, et al. Kinetics of normal hematopoietic stem and progenitor cells in a Notch1-induced leukemia model. *Blood*. (2009) 114:3783–92. doi: 10.1182/blood-2009-06-227843

19. Vago L, Gojo I. Immune escape and immunotherapy of acute myeloid leukemia. *J Clin Invest*. (2020) 130:1552–64. doi: 10.1172/JCI129204

20. Tang X, Wang Z, Wang J, Cui S, Xu R, Wang Y. Functions and regulatory mechanisms of resting hematopoietic stem cells: a promising targeted therapeutic strategy. *Stem Cell Res Ther*. (2023) 14:73. doi: 10.1186/s13287-023-03316-5

21. Zhang D, Gao X, Li H, Borger DK, Wei Q, Yang E, et al. The microbiota regulates hematopoietic stem cell fate decisions by controlling iron availability in bone marrow. *Cell Stem Cell*. (2022) 29:232–247. doi: 10.1016/j.stem.2021.12.009

22. Wang S, He X, Wu Q, Jiang L, Chen L, Yu Y, et al. Transferrin receptor 1-mediated iron uptake plays an essential role in hematopoiesis. *Haematologica*. (2020) 105:2071–82. doi: 10.3324/haematol.2019.224899

23. Talkhoncheh MS, Baudet A, Ek F, Subramaniam A, Kao Y-R, Miharada N, et al. Ciclopirox ethanolamine preserves the immature state of human HSCs by mediating intracellular iron content. *Blood Adv*. (2023) 7:7407–17. doi: 10.1182/bloodadvances.2023009844

24. Yi W, Zhang J, Huang Y, Zhan Q, Zou M, Cheng X, et al. Ferritin-mediated mitochondrial iron homeostasis is essential for the survival of hematopoietic stem cells and leukemic stem cells. *Leukemia*. (2024) 38:1003–18. doi: 10.1038/s41375-024-02169-y

25. Hu T, Cheng B, Matsunaga A, Zhang T, Lu X, Fang H, et al. Single-cell analysis defines highly specific leukemia-induced neutrophils and links MMP8 expression to recruitment of tumor associated neutrophils during FGFR1 driven leukemogenesis. *Exp Hematol Oncol*. (2024) 13:49. doi: 10.1186/s40164-024-00514-6

26. Li W, Wang F, Guo R, Bian Z, Song Y. Targeting macrophages in hematological Malignancies: recent advances and future directions. *J Hematol Oncol*. (2022) 15:110. doi: 10.1186/s13045-022-01328-x

27. Crinier A, Dumas P-Y, Escalière B, Piperoglou C, Gil L, Villacreces A, et al. Single-cell profiling reveals the trajectories of natural killer cell differentiation in bone marrow and a stress signature induced by acute myeloid leukemia. *Cell Mol Immunol*. (2021) 18:1290–304. doi: 10.1038/s41423-020-00574-8

28. Yang F, Wang R, Feng W, Chen C, Yang X, Wang L, et al. Characteristics of NK cells from leukemic microenvironment in MLL-AF9 induced acute myeloid leukemia. *Mol Immunol*. (2018) 93:68–78. doi: 10.1016/j.molimm.2017.11.003

29. Wang R, Feng W, Wang H, Wang L, Yang X, Yang F, et al. Blocking migration of regulatory T cells to leukemic hematopoietic microenvironment delays disease progression in mouse leukemia model. *Cancer letters*. (2020) 469:151–61. doi: 10.1016/j.canlet.2019.10.032

30. Chen S-Y, Yang X, Feng W-L, Liao J-F, Wang L-N, Feng L, et al. Organ-specific microenvironment modifies diverse functional and phenotypic characteristics of leukemia-associated macrophages in mouse T cell acute lymphoblastic leukemia. *J Immunol (Baltimore Md: 1950)*. (2015) 194:2919–29. doi: 10.4049/jimmunol.1400451

31. Yang X, Feng W, Wang R, Yang F, Wang L, Chen S, et al. Repolarizing heterogeneous leukemia-associated macrophages with more M1 characteristics eliminates their pro-leukemic effects. *Oncoimmunology*. (2018) 7:e1412910. doi: 10.1080/2162402X.2017.1412910

32. Yang F, Feng W, Wang H, Wang L, Liu X, Wang R, et al. Monocyte-derived leukemia-associated macrophages facilitate extramedullary distribution of T-cell acute lymphoblastic leukemia cells. *Cancer Res*. (2020) 80:3677–91. doi: 10.1158/0008-5472.CAN-20-0034

33. Jais A, Einwallner E, Sharif O, Gossens K, Lu TT, Soyal SM, et al. Heme oxygenase-1 drives metaflammation and insulin resistance in mouse and man. *Cell*. (2014) 158:25–40. doi: 10.1016/j.cell.2014.04.043

34. Handa P, Thomas S, Morgan-Stevenson V, Maliken BD, Gochanour E, Boukhar S, et al. Iron alters macrophage polarization status and leads to steatohepatitis and fibrogenesis. *J leukocyte Biol*. (2019) 105:1015–26. doi: 10.1002/JLB.3A0318-108R

35. Joffin N, Gliniak CM, Funcke J-B, Paschoal VA, Crewe C, Chen S, et al. Adipose tissue macrophages exert systemic metabolic control by manipulating local iron concentrations. *Nat Metab*. (2022) 4:1474–94. doi: 10.1038/s42255-022-00664-z

36. Kao J-K, Wang S-C, Ho L-W, Huang S-W, Lee C-H, Lee M-S, et al. M2-like polarization of THP-1 monocyte-derived macrophages under chronic iron overload. *Ann hematol*. (2020) 99:431–41. doi: 10.1007/s00277-020-03916-8

37. Sun J-L, Zhang N-P, Xu R-C, Zhang G-C, Liu Z-Y, Abuduwaili W, et al. Tumor cell-imposed iron restriction drives immunosuppressive polarization of tumor-associated macrophages. *J Transl Med*. (2021) 19:347. doi: 10.1186/s12967-021-03034-7

38. Wilkinson HN, Roberts ER, Stafford AR, Banyard KL, Matteucci P, Mace KA, et al. Tissue iron promotes wound repair via M2 macrophage polarization and the chemokine (C-C motif) ligands 17 and 22. *Am J pathology*. (2019) 189:2196–208. doi: 10.1016/j.ajpath.2019.07.015

39. Zhang D, Cui X, Li Y, Wang R, Wang H, Dai Y, et al. Sox13 and M2-like leukemia-associated macrophages contribute to endogenous IL-34 caused accelerated progression of acute myeloid leukemia. *Cell Death Dis*. (2023) 14:308. doi: 10.1038/s41419-023-05822-z

40. Weber S, Parmon A, Kurrle N, Schnütgen F, Serve H. The clinical significance of iron overload and iron metabolism in myelodysplastic syndrome and acute myeloid leukemia. *Front Immunol*. (2020) 11:627662. doi: 10.3389/fimmu.2020.627662

41. Cheng H. Deciphering the hematopoietic cell ecosystem. *Blood Sci*. (2024) 6: e00211. doi: 10.1097/BS9.0000000000000211

42. Tanaka H, Espinoza JL, Fujiwara R, Rai S, Morita Y, Ashida T, et al. Excessive reactive iron impairs hematopoiesis by affecting both immature hematopoietic cells and stromal cells. *Cells*. (2019) 8:226. doi: 10.3390/cells8030226

43. Lu W, Zhao M, Rajbhandary S, Xie F, Chai X, Mu J, et al. Free iron catalyzes oxidative damage to hematopoietic cells/mesenchymal stem cells *in vitro* and suppresses hematopoiesis in iron overload patients. *Eur J Haematol*. (2013) 91:249–61. doi: 10.1111/ejh.12159

44. Zeng X, Li X, Li X, Wei C, Shi C, Hu K, et al. Fecal microbiota transplantation from young mice rejuvenates aged hematopoietic stem cells by suppressing inflammation. *Blood*. (2023) 141:1691–707. doi: 10.1182/blood.2022017514

45. Abdelfattah A, Hughes-Davies A, Clayfield L, Menendez-Gonzalez JB, Almotiri A, Alotaibi B, et al. Gata2 haploinsufficiency promotes proliferation and functional decline of hematopoietic stem cells with myeloid bias during aging. *Blood Adv*. (2021) 5:4285–90. doi: 10.1182/bloodadvances.2021004726

46. Wu L, Lin Q, Chatla S, Amarachintha S, Wilson AF, Atale N, et al. LepR+ niche cell-derived AREG compromises hematopoietic stem cell maintenance under conditions of DNA repair deficiency and aging. *Blood*. (2023) 142:1529–42. doi: 10.1182/blood.2022018212

47. Mansell E, Sigurdsson V, Deltcheva E, Brown J, James C, Miharada K, et al. Mitochondrial potentiation ameliorates age-related heterogeneity in hematopoietic stem cell function. *Cell Stem Cell*. (2021) 28:241–256. doi: 10.1016/j.stem.2020.09.018

48. Zhang Q, Chen C, Zou X, Wu W, Di Y, Li N, et al. Iron promotes ovarian cancer Malignancy and advances platinum resistance by enhancing DNA repair via FTH1/FTL/POLQ/RAD51 axis. *Cell Death Dis*. (2024) 15:329. doi: 10.1038/s41419-024-06688-5

49. Moore JA, Mistry JJ, Hellmich C, Horton RH, Wojtowicz EE, Jibril A, et al. LC3-associated phagocytosis in bone marrow macrophages suppresses acute myeloid leukemia progression through STING activation. *J Clin Invest*. (2022) 132:e153157. doi: 10.1172/JCI153157

50. Zhang X, Li S, Malik I, Do MH, Ji L, Chou C, et al. Reprogramming tumour-associated macrophages to outcompete cancer cells. *Nature*. (2023) 619:616–23. doi: 10.1038/s41586-023-06256-5

51. Xia Y, Rao L, Yao H, Wang Z, Ning P, Chen X. Engineering macrophages for cancer immunotherapy and drug delivery. *Adv Mater*. (2020) 32:e2002054. doi: 10.1002/adma.202002054

52. Van Overmeire E, Laoui D, Keirsse J, Van Ginderachter JA, Sarukhan A. Mechanisms driving macrophage diversity and specialization in distinct tumor microenvironments and parallelisms with other tissues. *Front Immunol*. (2014) 5:127. doi: 10.3389/fimmu.2014.00127

53. Soares MP, Hamza I. Macrophages and iron metabolism. *Immunity*. (2016) 44:492–504. doi: 10.1016/j.immuni.2016.02.016

54. Wang J, Mi S, Ding M, Li X, Yuan S. Metabolism and polarization regulation of macrophages in the tumor microenvironment. *Cancer letters*. (2022) 543:215766. doi: 10.1016/j.canlet.2022.215766

55. Morrissey MA, Kern N, Vale RD. CD47 ligation repositions the inhibitory receptor SIRPA to suppress integrin activation and phagocytosis. *Immunity*. (2020) 53:290–302. doi: 10.1016/j.immuni.2020.07.008

56. McCracken MN, Cha AC, Weissman IL. Molecular pathways: activating T cells after cancer cell phagocytosis from blockade of CD47 "Don't eat me" Signals. *Clin Cancer Res*. (2015) 21:3597–601. doi: 10.1158/1078-0432.CCR-14-2520

57. Jaiswal S, Jamieson CHM, Pang WW, Park CY, Chao MP, Majeti R, et al. CD47 is upregulated on circulating hematopoietic stem cells and leukemia cells to avoid phagocytosis. *Cell*. (2009) 138:271–85. doi: 10.1016/j.cell.2009.05.046

58. Kasakovski D, Xu L, Li Y. T cell senescence and CAR-T cell exhaustion in hematological Malignancies. *J Hematol Oncol*. (2018) 11:91. doi: 10.1186/s13045-018-0629-x

59. Liu L, Cheng X, Yang H, Lian S, Jiang Y, Liang J, et al. BCL-2 expression promotes immunosuppression in chronic lymphocytic leukemia by enhancing regulatory T cell differentiation and cytotoxic T cell exhaustion. *Mol Cancer*. (2022) 21:59. doi: 10.1186/s12943-022-01516-w

60. Tracy SI, Venkatesh H, Hekim C, Heltemes-Harris LM, Knutson TP, Bachanova V, et al. Combining nilotinib and PD-L1 blockade reverses CD4+ T-cell dysfunction and prevents relapse in acute B-cell leukemia. *Blood*. (2022) 140:335–48. doi: 10.1182/blood.2021015341

61. Zhou Y-J, Li G, Wang J, Liu M, Wang Z, Song Y, et al. PD-L1: expression regulation. *Blood Sci*. (2023) 5:77–91. doi: 10.1097/BS9.0000000000000149

62. de Masson A, Darbord D, Dobos G, Boisson M, Roelens M, Ram-Wolff C, et al. Macrophage-derived CXCL9 and CXCL11, T-cell skin homing, and disease control in mogamulizumab-treated CTCL patients. *Blood*. (2022) 139:1820–32. doi: 10.1182/blood.2021013341

63. Hanna BS, McClanahan F, Yazdanparast H, Zaborsky N, Kalter V, Rößner PM, et al. Depletion of CLL-associated patrolling monocytes and macrophages controls disease development and repairs immune dysfunction *in vivo*. *Leukemia*. (2016) 30:570–9. doi: 10.1038/leu.2015.305